Vietnam Journal of Mechanics, Vietnam Academy of Science and Technology
DOI: https://doi.org/10.15625/0866-7136/24104

UNCOUPLED VIBRATIONS IN CRACKED FUNCTIONALLY GRADED BEAMS WITH TEMPERATURE-DEPENDENT PROPERTIES

Do Nam[1], **Nguyen Tien Long**[2], **Phi Thi Hang**[3], **Nguyen Tien Khiem**[4,*]
[1]*VNU University of Engineering and Technology, 144 Xuan Thuy, Cau Giay Ward, Hanoi, Vietnam*
[2]*Institute of Mechanics and Environment Engineering, VUSTA, 264 Doi Can, Ngoc Ha Ward, Hanoi, Vietnam*
[3]*Electric Power University, 235 Hoang Quoc Viet, Nghia Do Ward, Hanoi, Vietnam*
[4]*CIRTECH Institute, HUTECH University, 475A Dien Bien Phu, Thanh My Tay Ward, Ho Chi Minh City, Vietnam*
E-mail: nt.khiem55@hutech.edu.vn

Received: 17 January 2026 / Revised: 13 March 2026 / Accepted: 15 April 2026
Published online: 12 June 2026

Abstract. In the present study, the free vibration of cracked temperature-dependent functionally graded Euler–Bernoulli beams is addressed using the power law of material gradation and double spring model of a transverse open crack. Under the assumptions of ignoring inertia for rotation and axial deformation, discomposed longitudinal and bending vibrations are investigated for temperature-dependent multiple-cracked functionally graded beams. Hence, the effect of the material gradation index, temperature rise distribution, and cracks on the natural frequencies of the decoupled vibration modes is examined. Numerical results show that the longitudinal wave speed and the natural frequencies of both the longitudinal and bending vibrations decrease with an increasing material fraction index and temperature rise. It is also revealed that there is a significant effect of material gradation and temperature on the sensitivity of the beam natural frequencies to crack location and depth.

Keywords: functionally graded material, cracked beam, thermal effect, uncoupled vibration.

1. INTRODUCTION

Functionally Graded Material (FGM) is usually made of ceramics and metals with the aim of simultaneously increasing thermal protection and load-carrying capability of FGM structures working in a harsh thermal environment. Since 1984 when FGM was discovered in Japan as a novel composite, FGMs and FGM structures have become the subject of intensive research in the modeling and analysis of these structures. The essential results recently obtained on the subject are presented by Birman and Byrd (2007), Gayen et al. (2019), Gupta and Talha (2015), Singh and Sharma (2019), and Zahedinejad et al. (2020). A short overview given below is concerned with the vibration problem of functionally graded beam (FGB) structures subjected to thermal load and damage such as cracks.

Irrespective of which beam theory (Euler–Bernoulli, Timoshenko or higher-order shear deformation beam theories) is used for modeling FGBs, the longitudinal and bending vibration modes in an FGB have been affirmed to be coupled (Aydogdu & Taskin, 2007; Jin & Wang, 2015; Pradhan & Chakraverty, 2013; Su & Banerjee, 2015) except some cases. First, using Timoshenko functionally graded beams, Huyen and Khiem (2017) have proved that when

the so-called proportional condition ($E_t/\rho_t = E_b/\rho_b$) is fulfilled, longitudinal and bending vibrations are completely uncoupled. Second, under the assumption of no axial force applied, Li (2008) established purely bending equations of motion that are valid for the analysis of both Timoshenko's and Euler–Bernoulli functionally graded beams. However, in the latter study, the author did not account for the physical position of the neutral axis which may have a significant effect on the vibration of the FGB. The neutral axis position has been used for calculating the effective mass and stiffness of a functionally graded beam, the bending vibration for which is represented exactly in the same form as is well known for classical homogeneous Euler–Bernoulli beams (W. R. Chen & Chang, 2017). Though this approach is rather simple in the vibration analysis of FGBs, it has been validated by a good agreement in the comparison of natural frequencies calculated with such a simplified model and a standard one of FGBs. Moreover, the simple model was applied by Aydin (2013) and Yang and Chen (2008) for studying the purely bending vibration of cracked FGBs and it allows one to expose the typical effect of cracks on the natural frequencies of FGBs. Free vibration of cracked functionally graded beams was thoroughly investigated within the Timoshenko beam theory by Khiem et al. (2017) and Khiem (2022). However, axial and flexural vibration modes are still strongly coupled so that the behavior of the axial vibration mode has not been comprehensively investigated. Sherafatnia et al. (2014) have established equations for the vibration of cracked FGBs using various engineering beam theories such as the Euler–Bernoulli, Rayleigh and Timoshenko beams, but the axial vibration components are still not specifically examined. Thus, it can be noted here that most studies on the vibration of FGBs either ignore the longitudinal wave or keep it as an implicit vibration component, focusing major attention only on investigating the flexural mode. The present study aims at fulfilling this gap by investigating uncoupled longitudinal and flexural vibrations of cracked FGBs.

As FGM is usually made of ceramic and metal constituents to increase thermal resistance of the material, studying dynamical characteristics of FGM structures under thermal load is of great importance. The effect of temperature on the dynamics characteristics of FGM beams was studied in a wide literature, for instance, by Alshorbagy (2013), J. Chen et al. (2018), Gayen (2024), Hai et al. (2025), Mahi et al. (2010), and Trinh et al. (2016). Namely, Alshorbagy (2013) demonstrated that dimensionless natural frequencies decrease with an increase in both the material distribution index and temperature, and the temperature effect on high frequencies is greater than on the lower ones. Mahi et al. (2010) formulated the thermo-mechanical free vibration problem of symmetric FG beams based on different high-order shear deformation beam theories and various laws of material gradation such as the Power, Exponential and Sigmoid ones. J. Chen et al. (2018) investigated variations of the fundamental frequency of FGM beams with general boundary conditions based on the different high-order shear deformation beam theories and various temperature distributions including the uniform, linear, and nonlinear distributions across the beam thickness. Both the free vibration and thermal buckling of FGM beams were studied by Gayen (2024) and Trinh et al. (2016), where Gayen (2024) concluded that the material and temperature parameters have a comparatively high impact on the thermo-elastic behavior of circular FG beams. Trinh et al. (2016) demonstrated that temperature dependent solutions are significantly lower than those of temperature independent ones, especially for thick beams. The effect of neutral axis position on vibration of temperature-dependent functionally graded beams has been examined recently by Hai et al. (2025), who stated that not only actual position of neutral axis but also nonlinear distribution of temperature field should be considered if the temperature change amount is greater than 800 K. Concerning cracked FGM structures under thermal load, to the authors' knowledge, there are some published studies on the vibration of cracked FGM plates (Minh & Duc, 2021; Natarajan et al., 2011) and micro- and nano-beams (Aria et al., 2019; Esen et al., 2021). Elaikh and Agboola (2022) investigated the transverse vibration characteristics of a cracked axially moving functionally graded beam under thermal load and Huyen et al. (2025)

studied the coupled effect of cracks and temperature on the natural frequencies of functionally graded Timoshenko beams. In the latter work, both axial and flexural compliances of the double spring crack model have been studied in dependence upon not only the material gradient index but also the temperature rise. Nevertheless, to the authors' knowledge, uncoupled vibration modes in cracked functionally graded Euler–Bernoulli beams with temperature-dependent properties have not been found in the published literature.

Thus, in the present study, the free vibration problem is formulated and solved for cracked temperature-dependent functionally graded Euler–Bernoulli beams using the power law of material gradation and a double spring model of a transverse open crack. Under the assumptions of ignoring inertia for rotation and axial deformation, discomposed longitudinal and bending vibrations are investigated for temperature-dependent multiple-cracked functionally graded beam. Hence, the effect of the material gradation index, temperature rise distribution and cracks on the natural frequencies of the longitudinal and bending vibration modes is examined. Numerical results show that the longitudinal wave speed and the natural frequencies of both the longitudinal and bending vibrations decrease with an increasing material fraction index and temperature rise. It is also revealed that there is a significant effect of material gradation and temperature on the sensitivity of the beam natural frequencies to crack location and depth.

2. MODEL OF TEMPERATURE-DEPENDENT CRACKED FUNCTIONALLY GRADED BEAMS

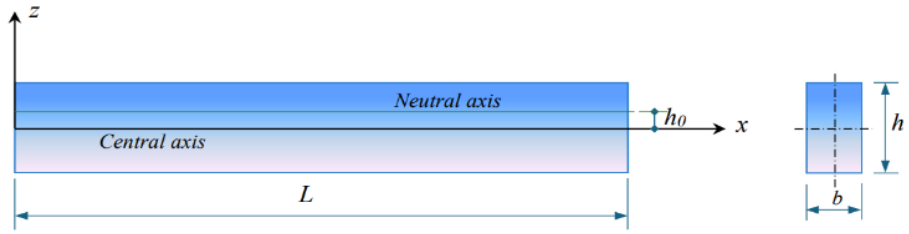

Fig. 1. Model of functionally graded beam

Consider a beam of length ℓ, cross-section area $A = b \times h$, as shown in Fig. 1, that is made of FGM with material properties varying along the thickness by the power law

$$P(z,T) = P_b(T) + [P_t(T) - P_b(T)](z/h + 1/2)^p, \quad -h/2 \leqslant z \leqslant h/2, \tag{1}$$

where P stands for E, G and ρ, the elasticity, shear modulus and material density at the top (with index t) and bottom (with index b) respectively; z is the ordinate from the central axis, T is the temperature field. The dependence of material properties on temperature is defined by

$$P(T) = P_0\left[P_{-1}T^{-1} + 1 + P_1T + P_2T^2 + P_3T^3\right], \tag{2}$$

with coefficients $P_0, P_{-1}, P_1, P_2, P_3$ given specifically for material constituents (Table 1).

According to the Euler–Bernoulli beam theory, when shear deformation is ignored, the displacement field in the cross-section at x is represented by

$$u(x,z,t) = u_0(x,t) - (z - h_0)\partial w_0(x,t)/\partial x, \quad w(x,z,t) = w_0(x,t), \tag{3}$$

with $u_0(x,t), w_0(x,t)$ are displacements of neutral axis located at the high h_0 from the central axis that is determined by Huyen and Khiem (2017) as

$$h_0 = \int_{-h/2}^{h/2} E(z,T)z\mathrm{d}z \Big/ \int_{-h/2}^{h/2} E(z,T)\mathrm{d}z. \tag{4}$$

Table 1. Temperature dependent materials constants (Alshorbagy, 2013)

Material	Properties	P_0	P_{-1}	P_1	P_2	P_3
Si_3N_4	E (Pa)	$348.43e^{+9}$	0	$-3.070e^{-4}$	$1.260e^{-7}$	$-8.946e^{-11}$
	ν	0.24	0	0	0	0
	α (K^{-1})	$5.823e^{-6}$	0	$9.095e^{-4}$	0	0
	ρ (kg/m^3)	2370	0	0	0	0
	k	9.19	0	0	0	0
SUS304	E (Pa)	$2.01e^{+11}$	0	$3.08e^{-4}$	$-6.534e^{-7}$	0
	ν	0.3262	0	$-2.002e^{-4}$	$3.797e^{-7}$	0
	α (K^{-1})	$1.233e^{-5}$	0	$8.086e^{-4}$	0	0
	ρ (kg/m^3)	8166	0	0	0	0
	k	12.04	0	0	0	0
Al_2O_3	E (Pa)	$349.55e^{+9}$	0	$-3.853e^{-4}$	$4.027e^{-7}$	$-1.673e^{-10}$
	ν	0.26	0	0	0	0
	α (K^{-1})	$6.826e^{-6}$	0	$1.838e^{-4}$	0	0
	ρ (kg/m^3)	3800	0	0	0	0
	k	-14.087	0	0	0	0
Zirconia	E (Pa)	$244.27e^{+9}$	0	$-1.371e^{-3}$	$1.214e^{-6}$	$-3.681e^{-10}$
	ν	0.2882	0	$1.133e^{-4}$	0	0
	α (K^{-1})	$12.766e^{-6}$	0	$-1.491e^{-3}$	$1.006e^{-5}$	$-6.778e^{-11}$
	ρ (kg/m^3)	5680	0	0	0	0
	k	9.19	0	0	0	0

Therefore, the constitutive equations take the form

$$\varepsilon_x = \frac{\partial u_0}{\partial x} - (z - h_0)\frac{\partial^2 w_0}{\partial x^2}, \quad \sigma_x = E(z,T)\varepsilon_x. \tag{5}$$

The stress due to the temperature rise is

$$\sigma_x^T = -E\,(z,T)\,\alpha\,(z,T)\,\delta T, \tag{6}$$

where $a(z,T)$ is the thermal expansion coefficient and δT is the distributed change in temperature defined in Appendix **A**.

Using the constitutive equations (3), (5) and (6), the strain and kinetic energies can be calculated as

$$\begin{aligned} U = U_s + U_T &= \frac{1}{2}\iiint \sigma_x\varepsilon_x \mathrm{d}V + \frac{1}{2}\iiint \sigma_x^T(u_{0,x}^2 + w_{0,x}^2)\mathrm{d}V \\ &= \frac{1}{2}\int_0^L A_{11}u_{0,x}^2 - 2A_{12}u_{0,x}w_{0,xx} + A_{22}w_{0,xx}^2 - A_T(u_{0,x}^2 + w_{0,x}^2)]\mathrm{d}x, \end{aligned} \tag{7}$$

$$K = \frac{1}{2}\int_0^L \left[I_{11}\left(\dot{u}_0^2 + \dot{w}_0^2\right) - 2I_{12}\dot{u}_0\dot{w}_{0,x} + I_{22}\dot{w}_{0,x}^2\right]\mathrm{d}x, \tag{8}$$

where $u_{0,x} = \partial u_0/\partial x, w_{0,x} = \partial w_0/\partial x, w_{0,xx} = \partial^2 w_0/\partial x^2, \dot{u}_0 = \partial u_0/\partial t, \dot{w}_0 = \partial w_0/\partial t, \ldots$, and

$$\{A_{11}, A_{12}, A_{22}\} = b\int_{-h/2}^{h/2} E(z,T)\left\{1, z-h_0, (z-h_0)^2\right\}\mathrm{d}z,$$
$$\{I_{11}, I_{12}, I_{22}\} = b\int_{-h/2}^{h/2} \rho(z), z-h_0, (z-h_0)^2\mathrm{d}z, \tag{9}$$

$$A_T = b\int_{-h/2}^{h/2} E(z,T)\,\alpha(z,T)\,\delta T(z)\,\mathrm{d}z. \tag{10}$$

Now, using the Hamilton principle allows one to derive the equations of motion for the beam in the form

$$I_{11}\ddot{u}_0 - I_{12}\ddot{w}_{0,x} - (A_{11} - A_T)u_{0,xx} + A_{12}w_{0,xxx} = 0,$$
$$I_{11}\ddot{w}_0 - I_{12}\ddot{u}_{0,x} + I_{22}\ddot{w}_{0,xx} - A_{12}u_{0,xxx} + A_{22}w_{0,xxxx} - A_T w_{0,xx} = 0. \tag{11}$$

By the Fourier transformation

$$\{U(x,\omega), W(x,\omega)\} = \int_{-\infty}^{\infty}\{u_0(x,t), w_0(x,t)\}\,e^{-i\omega t}\mathrm{d}t.$$

Eq. (11) becomes

$$(A_{11} - A_T)U''_{xx} + \omega^2 I_{11}U - A_{12}W'''_{xxx} - \omega^2 I_{12}W'_x = 0,$$
$$A_{22}W^{(\mathrm{IV})}_{xxxx} - \left(\omega^2 I_{22} + A_T\right)W''_{xx} - \omega^2 I_{11}W - A_{12}U'''_{xxx} + \omega^2 I_{12}U'_x = 0. \tag{12}$$

Furthermore, suppose that the beam contains an open transverse crack at the positions $e_j, j = 1, 2, \ldots, n$ and the crack is modeled as shown in Fig. 2 by a pair of springs of stiffness T, R. For the crack model the solution of Eq. (11) must satisfy the following conditions at the crack positions (Khiem & Lien, 2001)

$$U(e_j + 0) = U(e_j - 0) + \gamma_{aj}U'_x(e_j), \quad U'_x(e_j + 0) = U'_x(e_j - 0), \tag{13}$$
$$W(e_j + 0) = W(e_j - 0), \quad W''_{xx}(e_j + 0) = W''_{xx}(e_j - 0),$$
$$W'_x(e_j + 0) = W'_x(e_j - 0) + \gamma_{bj}W''_{xx}(e_j), \quad W'''_{xxx}(e_j + 0) = W'''_{xxx}(e_j - 0), \tag{14}$$

where

$$\gamma_{aj} = A_{11}/T_j, \quad \gamma_{bj} = A_{22}/R_j, \tag{15}$$

are the so-called axial and rotational compliances of the crack that could be calculated from the crack depth as follows.

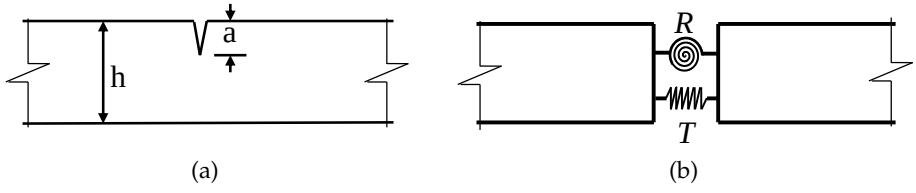

Fig. 2. Model of open edge crack in FGM beam

Note that in the case of a homogeneous temperature-independent beam the crack compliance is denoted by γ_a, γ_b and calculated as

$$\nu_a = E_0 A/T = 2\pi(1-\nu_0^2)h_b f_a(a/h_b), \quad \nu_b = E_0 I/R = 6\pi(1-\nu_0^2)h_b f_b(a/h_b), \tag{16}$$

where E_0, A, I are the Young's modulus, cross section area and moment of inertia of the homogeneous beam respectively and the functions $f_a(z), f_b(z)$ are given by Chondros et al. (1998a, 1998b)

$$\begin{aligned} f_a(z) &= z^2(0.6272 - 0.17248z + 5.92134z^2 - 10.7054z^3 + 31.5685z^4 - 67.47z^5 \\ &\quad + 139.123z^6 - 146.682z^7 + 92.3552z^8), \end{aligned} \tag{17}$$

$$\begin{aligned} f_b(z) &= z^2(0.6272 - 1.04533z + 4.5948z^2 - 9.9736z^3 + 20.2948z^4 - 33.0351z^5 \\ &\quad + 47.1063z^6 - 40.7556z^7 + 19.6z^8). \end{aligned} \tag{18}$$

Using the notation $E_0 = (E_0^t + E_0^b)/2$ the FGM beam's crack compliance can be rewritten as

$$\begin{aligned} \gamma_a &= (A_{11}/E_0A)(E_0A/T) = \varphi_a\left(p, E_r^t, E_r^b\right)\nu_a(a), \\ \gamma_b &= (A_{22}/E_0I)(E_0I/R) = \varphi_b\left(p, E_r^t, E_r^b\right)\nu_b(a), \end{aligned} \tag{19}$$

with the notations

$$\varphi_a\left(p, E_r^t, E_r^b\right) = A_{11}\left(p, E_r^t, E_r^b\right)/E_0A, \quad \varphi_b\left(p, E_r^t, E_r^b\right) = A_{22}\left(p, E_r^t, E_r^b\right)/E_0I. \tag{20}$$

3. FREE VIBRATION OF CRACKED FUNCTIONALLY GRADED EULER-BERNOULLI BEAMS

Since the exact position of the neutral axis has been determined from condition (4) that simply results in $A_{12} = 0$. Additionally, the inertia terms of rotation $\ddot{\omega}_{0,x}$ and axial strain $\ddot{u}_{0,x}$ are usually ignored in the Euler–Bernoulli theory, so that the equations (12) would be reduced to

$$(A_{11} - A_T)U''_{xx} + \omega^2 I_{11}U = 0, \tag{21}$$

$$A_{22}W^{(IV)}_{xx} + \left(\omega^2 I_{22} - A_T\right)W''_{xx} - \omega^2 I_{11}W = 0. \tag{22}$$

The equations show that the longitudinal and bending vibrations of functionally graded Euler–Bernoulli beams are decoupled, and Eq. (21) and Eq. (22) can be separately investigated. In the case of multiple cracked beams, the solution of Eq. (21) is subjected to conditions (13) and the solution of Eq. (22) is subjected to conditions (14).

3.1. Longitudinal vibration

First, the equation of longitudinal vibration in beams (21) can be rewritten as

$$U''_{xx} + \lambda^2 U = 0, \quad \lambda = \sqrt{(I_{11}/(A_{11} - A_T))}, \tag{23}$$

that describes the elastic wave propagating in a functionally graded rod. The equation should be solved in combination with boundary conditions and conditions (13) in the case of cracked beams.

Next, for finding the general solution of Eq. (23) satisfying conditions (13), it can be proved that an arbitrary solution of Eq. (23) satisfying conditions (13) is represented as

$$L(x) = L_0(x) + \sum_{j=1}^{n} \mu_{aj} K(x - e_j), \tag{24}$$

where $L_0(x)$ is a continuous solution of Eq. (23) without cracks, and $K(x)$ is the function

$$K(x) = \begin{cases} \cos(\lambda x), & \text{for } x \geq 0, \\ 0, & \text{for } x < 0, \end{cases} \quad K'(x) = -\lambda \begin{cases} \sin(\lambda x), & \text{for } x \geq 0, \\ 0, & \text{for } x < 0. \end{cases} \tag{25}$$

and

$$\mu_{aj} = \gamma_{aj}\left[L'_0(e_j) - \lambda \sum_{k=1}^{j-1} \mu_k \sin\lambda(e_j - e_k)\right]. \tag{26}$$

Namely, since $\cos\lambda x, \sin\lambda x$ and $L_0(x)$ are all solutions of Eq. (23), the expression (24) is a solution of that equation everywhere in the beam span $(0,\ell)$ except at the crack locations $e_j, j = 1,2,\ldots,n$, where the following conditions must be satisfied:

$$L(e_j+0) = L_0(e_j-0) + \gamma_{aj}L'(e_j), \quad L'(e_j+0) = L'(e_j-0). \tag{27}$$

Noting that for a continuous function $L_0(x)$ we have $L_0(e_j+0) = L_0(e_j-0) = L_0(e_j)$. Therefore, using Eq. (24) we can calculate

$$L'(e_j+0) = L_0'(e_j) + \sum_{k=1}^{j}\mu_{ak}K'(e_j+0-e_k) = L_0'(e_j) - \lambda\sum_{k=1}^{j-1}\mu_{ak}\sin\lambda(e_j-e_k) = L'(e_j-0),$$

and

$$L(e_j+0) = L_0(e_j) + \sum_{k=1}^{j}\mu_{ak}K\left(e_j+0-e_k\right) = L_0(e_j) - \lambda\sum_{k=1}^{j-1}\mu_{ak}\cos\lambda\left(e_j-e_k\right) + \mu_{aj}$$

$$= L(e_j-0) + \gamma_{aj}\left[L_0'(e_j) - \lambda\sum_{k=1}^{j-1}\mu_{ak}\sin\lambda(e_j-e_k)\right] = L(e_j-0) + L(e_j-0) + \gamma_{aj}L(e_j)'.$$

So, conditions (27) have been proved, and the expression (24) is really a solution of Eq. (23) satisfying conditions (13) at the crack locations.

On the other hand, it is obvious that the functions $\cos\lambda x, \sin\lambda x$ are independent continuous solutions of Eq. (23), so that putting these functions into (24) instead of the solution $L_0(x)$ yields two functions

$$L_1(x) = \cos\lambda x + \textstyle\sum_{j=1}^{n}\mu_{1j}K\left(x-e_j\right), \quad L_2(x) = \sin\lambda x + \textstyle\sum_{j=1}^{n}\mu_{2j}K\left(x-e_j\right), \tag{28}$$

with function $K(x)$ defined in (24) and

$$\mu_{1j} = -\lambda\gamma_{aj}\left[\sin\lambda e_j + \textstyle\sum_{k=1}^{j-1}\mu_{1k}\sin\lambda\left(e_j-e_k\right)\right], \; \mu_{2j} = \lambda\gamma_{aj}\left[\cos\lambda e_j - \textstyle\sum_{k=1}^{j-1}\mu_{2k}\sin\lambda\left(e_j-e_k\right)\right]. \tag{29}$$

Note, the so-called damage index vectors $\boldsymbol{\mu}_i = \{\mu_{i1},\ldots,\mu_{in}\}^T, i = 1,2$ can be calculated as

$$\boldsymbol{\mu}_i = \mathbf{A}^{-1}\mathbf{b}_i, \tag{30}$$

where

$$\mathbf{b}_1 = -\lambda\{\gamma_{a1}\sin\lambda e_1,\ldots,\gamma_{an}\sin\lambda e_n\}^T, \quad \mathbf{b}_2 = \lambda\{\gamma_{a1}\cos\lambda e_1,\ldots,\gamma_{an}\cos\lambda e_n\}^T,$$
$$\mathbf{A} = \left[a_{jk} = 1, j = k; a_{jk} = 0, k > j; a_{jk} = \lambda\sin\lambda\left(e_j-e_k\right), k < j, j,k = 1,\ldots,n\right].$$

Thus, the general solution of Eq. (23) satisfying conditions (13) is found in the form

$$U(x,\omega) = AL_1(x) + BL_2(x), \tag{31}$$

where A, B are constants determined from the given boundary conditions and the functions $L_1(x), L_2(x)$ are determined by Eqs. (24)–(26). This is the general shape of the longitudinal vibration of cracked beams that can be used for deriving the frequency equation as follows.

Assuming the boundary conditions for the vibrating beams are given by $U^{(p)}(0,\omega) = 0; U^{(q)}(\ell,\omega) = 0$, which allow one to obtain the frequency equation in the form

$$L_1^{(p)}(0,\omega)\,L_2^{(q)}(\ell,\omega) - L_2^{(p)}(0,\omega)\,L_1^{(q)}(\ell,\omega) = 0, \tag{32}$$

$L^{(p)}, L^{(q)}$ denote the p,q-order derivatives of the function $L(x,\omega)$ with respect to x. For example, the frequency equation for cantilever beams is

$$\cos\lambda\ell - \sum_{j=1}^{n}\mu_{2j}\sin\lambda\left(\ell-e_j\right) = 0. \tag{33}$$

Obviously, the effect of crack position and depth appears through the damage indexes μ_{ik}, while the material and temperature affect the beam's natural frequencies sought from Eq. (32) via the constants A_{11} and I_{11} calculated by Eq. (9).

3.2. Bending vibration

Note first that seeking the solution of Eq. (22) in the form $W(x,\omega) = Ce^{kx}$ allows for obtaining four independent continuous (without cracks) solutions of the equation as

$$\phi_{01}(x,\omega) = \cosh k_1 x,\ \phi_{02}(x,\omega) = \sinh k_1 x,\ \phi_{03}(x,\omega) = \cos k_2 x,\ \phi_{04}(x,\omega) = \sin k_2 x, \quad (34)$$

where

$$k_1 = \left\{ \left[\sqrt{\left(\omega^2 I_{22} - A_T\right)^2 + 4\omega^2 I_{11} A_{22}} - \left(\omega^2 I_{22} - A_T\right) \right] / 2A_{22} \right\}^{1/2},$$

$$k_2 = \left\{ \left[\sqrt{\left(\omega^2 I_{22} - A_T\right)^2 + 4\omega^2 I_{11} A_{22}} + \left(\omega^2 I_{22} - A_T\right) \right] / 2A_{22} \right\}^{1/2}.$$

Now, by analogy to what was accomplished above for the longitudinal vibration, in the case of the bending vibration, we can prove also that any solution of Eq. (22) satisfying conditions (14) is represented in the form

$$\phi(x) = \phi_0(x) + \sum_{j=1}^{n} \mu_{bj} K\left(x - e_j\right), \quad (35)$$

where $\phi_0(x)$ is one of the continuous solutions (34) and

$$K(x) = \begin{cases} S(x), & \text{for } x \geq 0, \\ 0, & \text{for } x < 0, \end{cases} \quad K'(x) = \begin{cases} S'(x), & \text{for } x \geq 0, \\ 0, & \text{for } x < 0, \end{cases}$$

$$S(x) = \frac{1}{k_1^2 + k_2^2} \left(\frac{k_2^2}{k_1} \sinh k_1 x + \frac{k_1^2}{k_2} \sin k_2 x \right), \quad (36)$$

$$K''(x) = \begin{cases} S''(x), & \text{for } x \geq 0, \\ 0, & \text{for } x < 0, \end{cases} \quad K'''(x) = \begin{cases} S'''(x), & \text{for } x \geq 0, \\ 0, & \text{for } x < 0, \end{cases}$$

and

$$\mu_{bj} = \gamma_{bj} \left[\phi_0''(e_j) + \sum_{k=1}^{j-1} \mu_{bk} S''\left(e_j - e_k\right) \right]. \quad (37)$$

Therefore, substituting sequentially the functions (34) into (35) one would get four independent cracked solutions

$$\begin{aligned} \phi_1(x,\omega) &= \phi_{01} + \sum_{j=1}^{n} \mu_{1j} K\left(x - e_j\right), \quad \phi_2(x,\omega) = \phi_{02}(x,\omega) + \sum_{j=1}^{n} \mu_{2j} K\left(x - e_j\right), \\ \phi_3(x,\omega) &= \phi_{03} + \sum_{j=1}^{n} \mu_{3j} K\left(x - e_j\right), \quad \phi_4(x,\omega) = \phi_{04}(x,\omega) + \sum_{j=1}^{n} \mu_{4j} K\left(x - e_j\right), \end{aligned} \quad (38)$$

where

$$\mu_{ij} = \gamma_{bj} \left[\phi_{0i}''(e_j) + \sum_{k=1}^{j-1} \mu_{ik} S''(e_j - e_k) \right], \quad j = 1, \ldots, n, \quad i = 1,2,3,4. \quad (39)$$

Finally, the general solution of Eq. (22) satisfying conditions (14) at the crack locations can be represented as

$$W(x,\omega) = C_1\phi_1(x,\omega) + C_2\phi_2(x,\omega) + C_3\phi_3(x,\omega) + C_4\phi_4(x,\omega). \quad (40)$$

In this case, the damage index vectors (39) are also calculated by equation (30) but with the following matrices $\mathbf{b} = \left\{ \gamma_{b1}\phi_0''(e_1), \ldots, \gamma_{bn}\phi_0''(e_n) \right\}^T$ and $\mathbf{A} = \left[a_{jk}, j,k = 1, \ldots, n \right]$ with

$$a_{jk} = 1, j = k, \quad a_{jk} = 0, k > j, \quad a_{jk} = S''\left(e_j - e_k\right), k < j.$$

Applying the given boundary conditions for the solution (40) results in the frequency equations presented below for the conventional boundary conditions.

Namely, in the case of simply supported beams with the boundary conditions

$$W(0) = M(0) = W(L) = M(L) = 0,$$

one would have the equation

$$[\mathbf{B}(\omega)]\{\mathbf{C}\} = \{\mathbf{0}\}, \tag{41}$$

for determining the constant vector $\mathbf{C} = \{C_1, 2, C_3, C_4\}^T$, with the matrix

$$[\mathbf{B}(\omega)] = [\mathbf{B}_{SS}(\omega)] = \begin{bmatrix} 1 & 0 & 1 & 0 \\ k_1^2 & 0 & -k_2^2 & 0 \\ \phi_1(\ell,\omega) & \phi_2(\ell,\omega) & \phi_3(\ell,\omega) & \phi_4(\ell,\omega) \\ \phi_1''(\ell,\omega) & \phi_2''(\ell,\omega) & \phi_3''(\ell,\omega) & \phi_4''(\ell,\omega) \end{bmatrix}. \tag{42}$$

For the existence of a nontrivial vector $\mathbf{C}$, the following condition must be satisfied

$$\det[\mathbf{B}(\omega)] = 0, \tag{43}$$

that provides the so-called frequency equation for finding the natural frequencies $\omega_1, \omega_2, \omega_3, \ldots$ of the FGM beam. In the case of clamped beams with the boundary conditions $W(0) = W'(0) = W(L) = W'(L) = 0$, the matrix $\mathbf{B}(\omega)$ in Eq. (43) has the form

$$[\mathbf{B}_{CC}(\omega)] = \begin{bmatrix} 1 & 0 & 1 & 0 \\ 0 & k_1 & 0 & k_2 \\ \phi_1(\ell,\omega) & \phi_2(\ell,\omega) & \phi_3(\ell,\omega) & \phi_4(\ell,\omega) \\ \phi_1'(\ell,\omega) & \phi_2'(\ell,\omega) & \phi_3'(\ell,\omega) & \phi_4'(\ell,\omega) \end{bmatrix}. \tag{44}$$

For a cantilever beam, the matrix $\mathbf{B}(\omega)$ is

$$[\mathbf{B}_{CF}(\omega)] = \begin{bmatrix} 1 & 0 & 1 & 0 \\ 0 & k_1 & 0 & k_1 \\ \phi_1''(\ell,\omega) & \phi_2''(\ell,\omega) & \phi_3''(\ell,\omega) & \phi_4''(\ell,\omega) \\ \phi_1'''(\ell,\omega) & \phi_2'''(\ell,\omega) & \phi_3'''(\ell,\omega) & \phi_4'''(\ell,\omega) \end{bmatrix}. \tag{45}$$

4. NUMERICAL RESULTS AND DISCUSSION

4.1. Theory validation

First, for validation of the above proposed theory, the non-dimensional fundamental frequency, $\bar{\omega} = \omega\left(L^2/h\right)\sqrt{\rho_b/E_b}$, is computed for a temperature-independent FGM beam made of Al_2O_3 at the top and Al at the bottom. In this example, the frequency is computed along various volume fraction index p and slenderness (L/h) for Euler–Bernoulli beams with simply supported (SS) and clamped-clamped (CC) ends. Such computed results are then compared to those obtained by Su and Banerjee (2015) and Hai et al. (2025) for Timoshenko beams, all presented in Table 2. It is observed that the fundamental frequency of functionally graded beams, in general, increases with slenderness and decreases as the volume fraction index is growing. However, there is a noticeable discrepancy between both the frequencies computed for the same functionally graded Timoshenko beam presented by Su and Banerjee (2015) and Hai et al. (2025). This is because Su and Banerjee (2015) did not consider the actual position of the neutral axis in the FGM beam, while Hai et al. (2025) did use the actual neutral axis instead of the central one. It is clear from Table 2 the well-known fact that both Euler–Bernoulli and Timoshenko beam theories are equivalent to use for the vibration analysis of slender beams with $L/h \geq 20$. For short or thick beams the Euler–Bernoulli beam theory gives overestimated natural frequencies and the volume fraction index of FGM makes an insignificant effect on the discrepancy between natural frequencies computed using the different beam theories. The agreement of the beam theories applied for computing the natural frequencies of functionally graded beams with simply supported ends shows to be better than that of clamped end beams. Finally, it must be noted herein that the natural frequencies of functionally graded Timoshenko beams are computed

under the coupling of both axial and flexural vibration modes, which are uncoupled for the functionally graded beams considered in the framework of the Euler–Bernoulli beam theory. So, the discrepancy between natural frequencies computed by using the Euler–Bernoulli or Timoshenko beam theories may be caused by the coupling of axial and flexural vibration modes in functionally graded beams.

Table 2. Comparison of dimensionless fundamental frequency computed with Euler–Bernoulli and Timoshenko beam theories for simply supported (SS) and clamped–clamped (CC) FGM beams without crack

L/h	p (V.F.I)	0.1	0.2	0.5	1.0	2.0	5.0	10.0
Simply Supported (SS) Beam								
5	S&B (Su & Banerjee, 2015)	4.7840	4.5296	4.0590	3.6890	3.3906	3.1088	2.9510
	EBB (Present)	4.8397	4.5638	4.0191	3.5794	3.2780	3.1050	3.0211
	T-beam (Hai et al., 2025)	4.5213	4.4865	3.9244	3.4633	3.1462	2.9722	2.8916
10	S&B (Su & Banerjee, 2015)	5.0010	4.7348	4.2433	3.8586	3.5510	3.2608	3.0959
	EBB (Present)	4.9007	4.6233	4.0756	3.6321	3.3255	3.1454	3.0580
	T-beam (Hai et al., 2025)	4.9875	4.6929	4.1039	3.6212	3.2917	3.1158	3.0336
20	S&B (Su & Banerjee, 2015)	5.0613	4.7918	4.2943	3.9058	3.5957	3.3032	3.1363
	EBB (Present)	4.9163	4.6385	4.0901	3.6456	3.3377	3.1557	3.0674
	T-beam (Hai et al., 2025)	5.0479	4.7495	4.1531	3.6645	3.3316	3.1553	3.0728
Clamped–Clamped (CC) Beam								
5	S&B (Su & Banerjee, 2015)	9.3380	8.8467	7.9241	7.1772	6.5543	5.9699	5.6680
	EBB (Present)	10.9266	10.3023	9.0696	8.0756	7.3963	7.0093	6.8216
	T-beam (Hai et al., 2025)	9.2882	8.7588	7.7037	6.8251	6.1819	5.7621	5.5697
10	S&B (Su & Banerjee, 2015)	10.8270	10.5230	9.1864	8.3437	7.6610	7.0184	6.6638
	EBB (Present)	11.0977	10.4692	9.2281	8.2235	7.5295	7.1226	6.9251
	T-beam (Hai et al., 2025)	10.7968	10.1662	8.9065	7.8691	7.1457	6.7325	6.5403
20	S&B (Su & Banerjee, 2015)	11.3340	10.7310	9.6159	8.7425	8.0434	7.3844	7.0116
	EBB (Present)	11.1417	10.5122	9.2690	8.2617	7.5639	7.1518	6.9518
	T-beam (Hai et al., 2025)	11.3041	10.6381	9.3068	8.2147	7.4664	7.0623	6.8734

Notice: V.F.I – Volume fraction index; EBB – Euler–Bernoulli Beam; T-Beam – Timoshenko Beam

4.2. Effect of temperature and material distribution

As shown in Eqs. (21) and (22), the longitudinal (axial) vibration and bending (flexural) vibration in functionally graded beams are uncoupled when the Euler–Bernoulli beam theory is applied. Moreover, Eq. (21) shows an interesting fact that the natural frequency is decomposed into two factors, the first of which is the wave number (WN) λ and the second one is the so-called longitudinal wave speed (LWS), $c = \sqrt{(A_{11} - A_T)/I_{11}}$. Obviously, the wave number is determined from Eq. (29) which is dependent only on the boundary conditions and cracks occurring in the beam, while the LWS is completely determined by material properties such as the elasticity modulus, distributions of mass and material constituents as well as the temperature expansion coefficient. Therefore, the effect of cracks on the natural frequencies in the longitudinal vibration of functionally graded beams can be examined independently of material properties. The volume fraction index p and temperature T make an effect only on the wave speed (LWS). On the contrary, the material properties, thermal effects and cracks are all mutually affecting

the beam bending vibration through the so-called frequency equation (41). Thus, the numerical results provided below in Figs. 3–12 are obtained for a Si_3N_4/SUB304 FGM beam with the power law of distribution (1) and temperature-dependent properties (2).

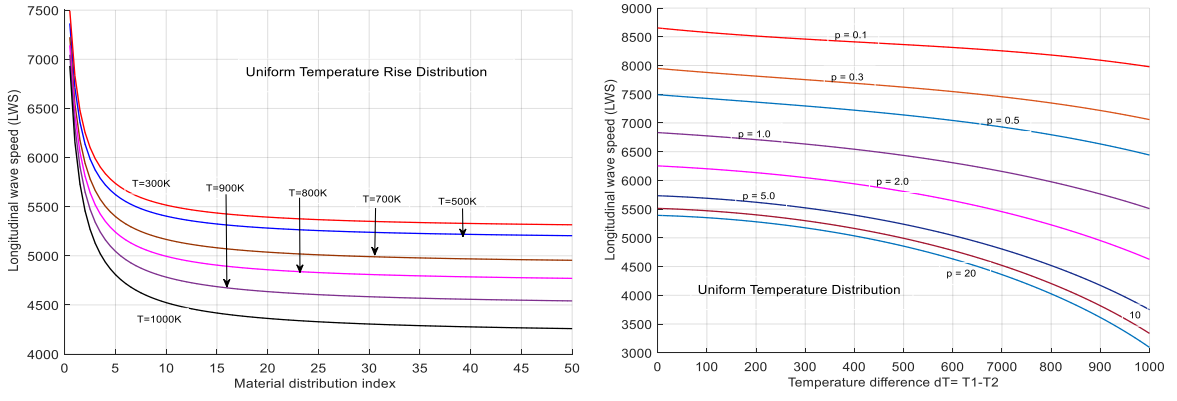

(a) UTD

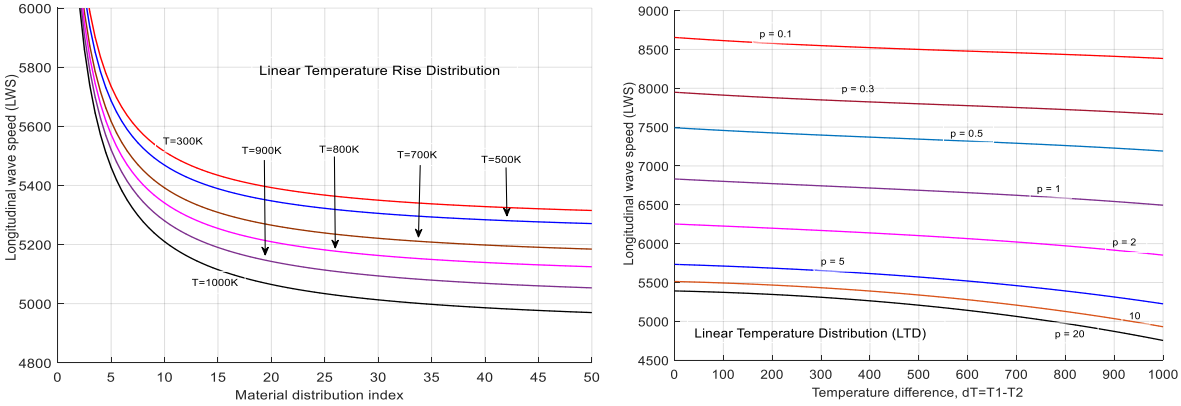

(b) LTD

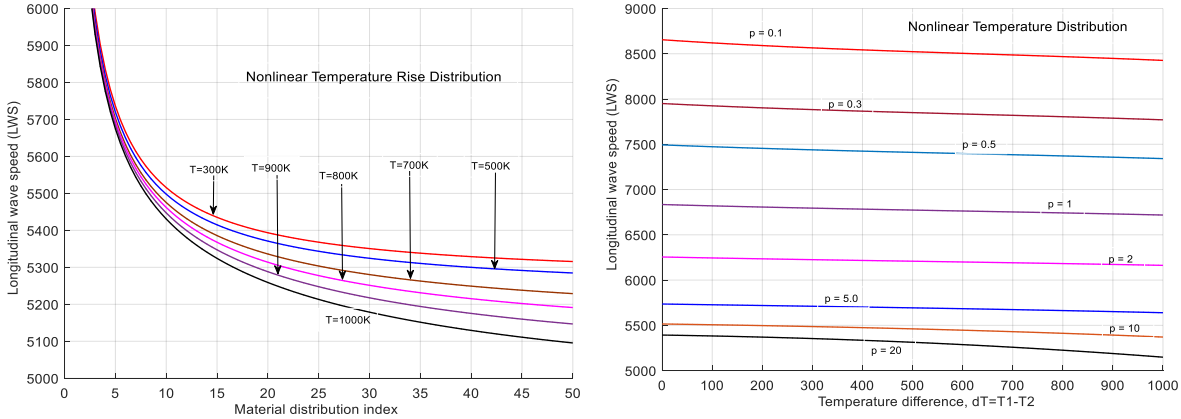

(c) NTD

Fig. 3. Effect of temperature rise and volume fraction index p on longitudinal wave speed of FGM beam

Fig. 3 exhibits the change in the longitudinal wave speed due to the volume fraction index (on the left) and temperature rise (on the right) in the cases of uniform, linear and nonlinear

temperature distributions, respectively. Visibly, the wave speed is reducing with an increasing material gradation index (p) and temperature difference ($\mathrm{d}T = T_{\mathrm{top}} - T_{\mathrm{bottom}}$) in all cases of temperature rise distributions. However, the rate of the LWS reduction is very different for material gradation and temperature rise. Namely, while the wave speed decreases almost linearly and slowly as the temperature changes, it is rapidly decreasing with an increasing material gradation index, especially when the material index is of a small value. Moreover, an increase in a uniformly distributed temperature reduces the wave speed more than linear and nonlinear distributions do, and a nonlinear temperature distribution has a less effect on the wave speed than the linear one.

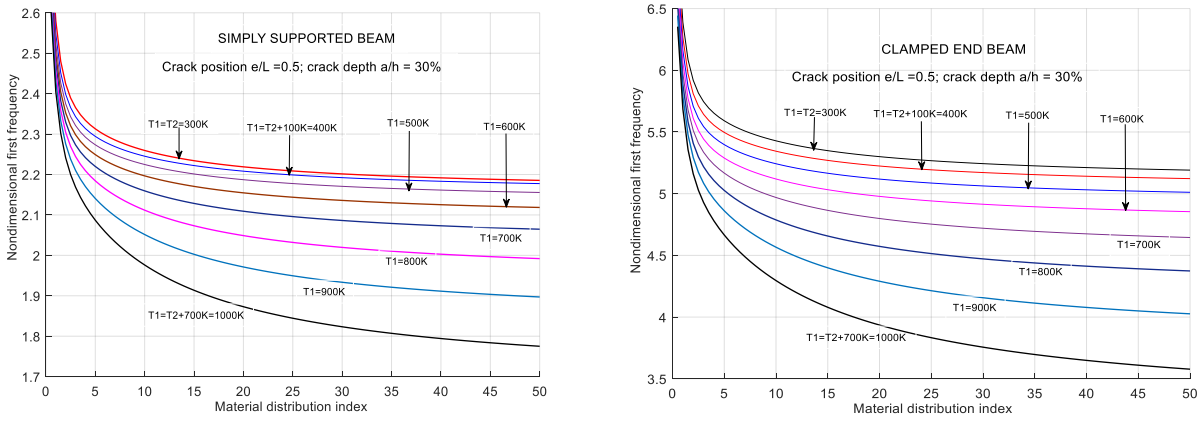

(a) SS-beam (b) CC-beam

Fig. 4. Bending fundamental frequency versus material gradation index in various generic temperatures of uniform distribution

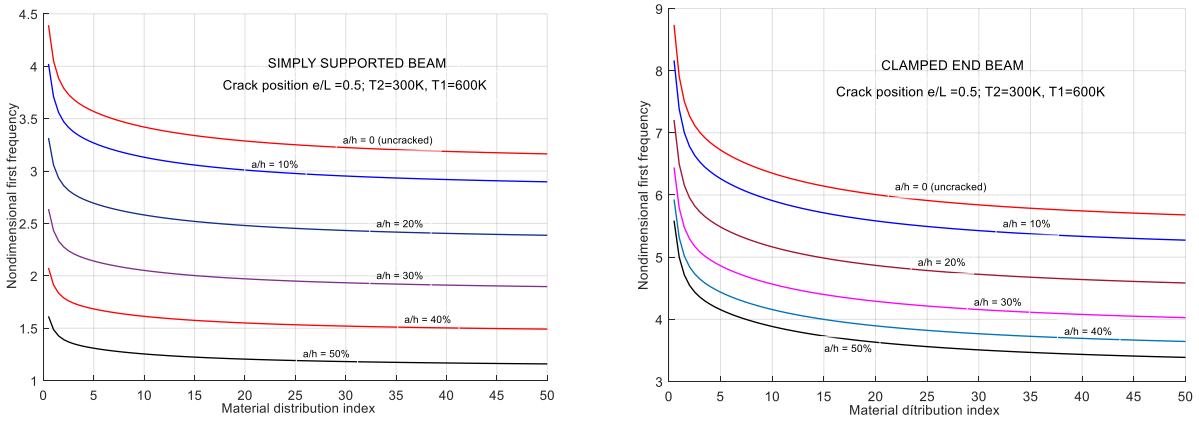

(a) Simply supported beam (b) Clamped end beam

Fig. 5. Bending fundamental frequency versus material distribution index in various crack depths

Figs. 4–7 present the fundamental frequency in the bending vibration of FGM beams with simply supported (SS) and clamped (CC) ends in dependence on the material gradation index, temperature rise and crack depth and location. Similarly to what was demonstrated above, the bending fundamental frequency of the beam is also reducing in the same manner as the number and speed of the longitudinal wave do, when the material gradation index, temperature

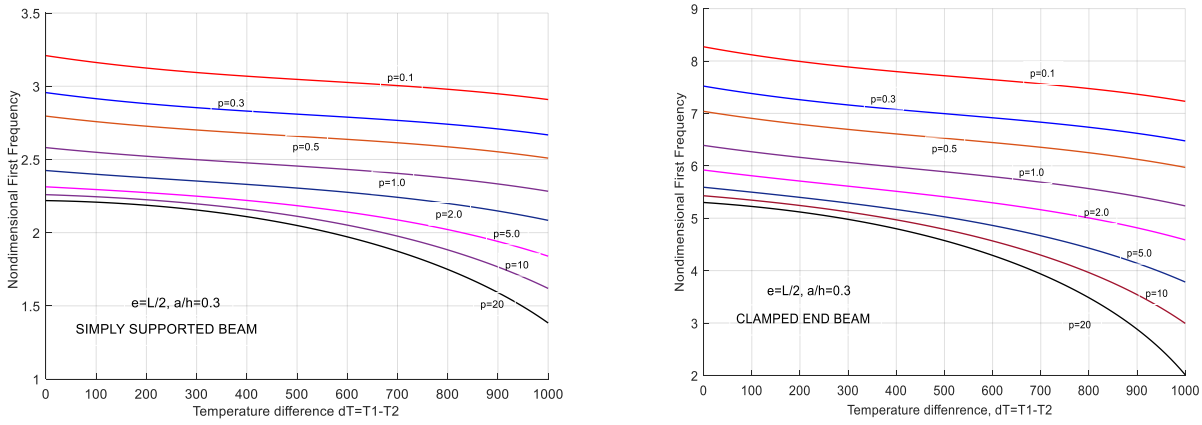

(a) Simply supported beam (b) Clamped end beam

Fig. 6. Bending fundamental frequency versus temperature in various material distribution index

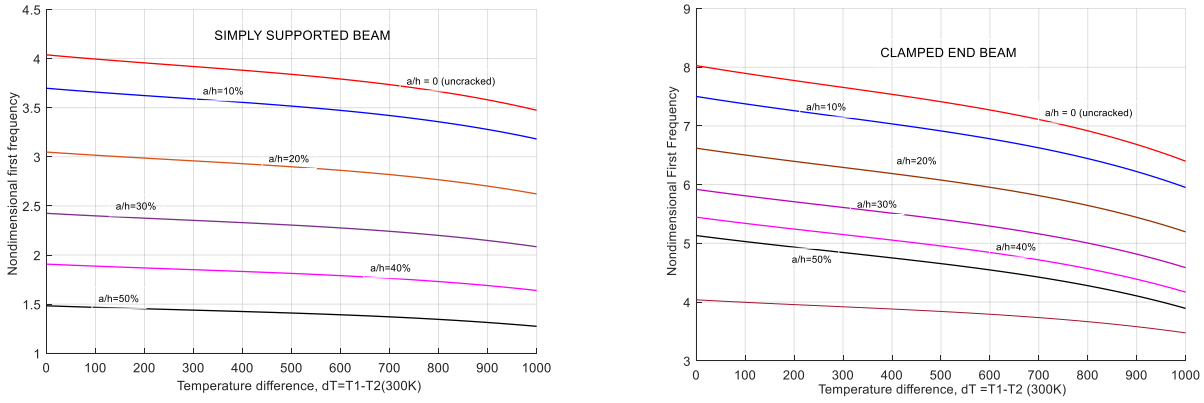

(a) Simply supported beam (b) Clamped end beam

Fig. 7. Bending fundamental frequency versus temperature in various material distribution index

and crack depth increase. A noticeable difference between the variations of longitudinal and bending frequencies along the material gradation index and temperature rise can be observed in that the bending frequency of a simply supported beam is slower varying than that of a clamped end beam. This may be explained by the fact that a simply supported beam has more freedom degrees in vibration compared to a beam with clamped ends, while the variation of the longitudinal wave speed is independent of boundary conditions.

4.3. Crack-induced change in natural frequencies of FGM beam

In this subsection, first, the natural frequency of a cracked beam normalized by that of an uncracked one is examined against crack parameters such as its location and depth. This nondimensional quantity is usually called the sensitivity of a natural frequency to a crack and is constrained by 0 and 1. Its maximum value equal to 1 implies that the beam is uncracked or the crack is not affecting the frequency. The natural frequency sensitivity to a crack is a useful indicator for studying and using crack-induced changes in natural frequencies for crack detection problems. However, as shown below, the characteristic is not convenient in examining the variation of frequencies due to other phenomena such as material properties including the temperature change. In such cases, the original values of frequencies are examined.

Fig. 8 demonstrates the effect of crack position and depth on the wave number related to the fundamental frequency of the longitudinal vibration in an FGM beam with different cases of boundary conditions. Obviously, an increase in crack depth leads to a decrease in the wave number except at the middle position on a beam with axial displacements fixed at its ends, where an occurred crack makes no effect on the wave number. In Figs. 9 and 10, there is depicted the sensitivity of the bending fundamental frequency to cracks in various distributions of temperature rise for simply supported and clamped end beams. Fig. 9 shows numerous curves representing the crack-induced change in the bending fundamental frequency of FGM beams against crack location and depth under uniformly distributed room temperature.

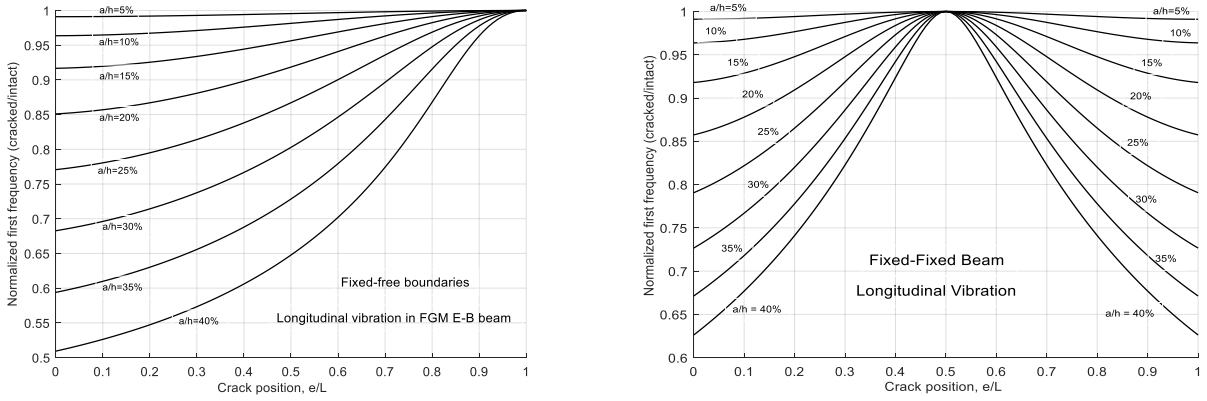

(a) Fixed-free beam (b) Fixed-fixed beams

Fig. 8. Effect of crack on wave number of FGM beams

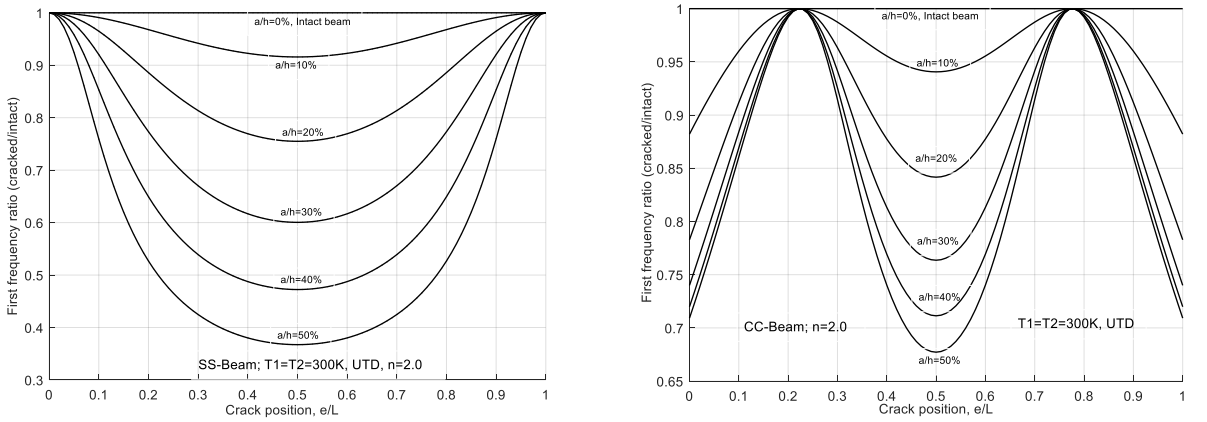

(a) SS-beam (b) CC-beam

Fig. 9. Sensitivity of bending fundamental frequency to crack in case of Uniform Temperature Distribution ($T_1 = T_2 = 300$ K)

As is well-known, the most sensitive crack location is the middle of both the SS-beam and CC-beam, and the unaffected crack locations are 0.22 and 0.78 for the CC-beam and the two ends (0 & 1) for the SS-beam. It can be observed from the Figure that the bending vibration frequency of FGM beams is much more sensitive to cracks than that of purely steel beams. This may be a contribution of the ceramic constituent into the FGM properties. Furthermore, it can be noted from Fig. 10 that in the case of an SS-beam the frequency sensitivity to a crack computed

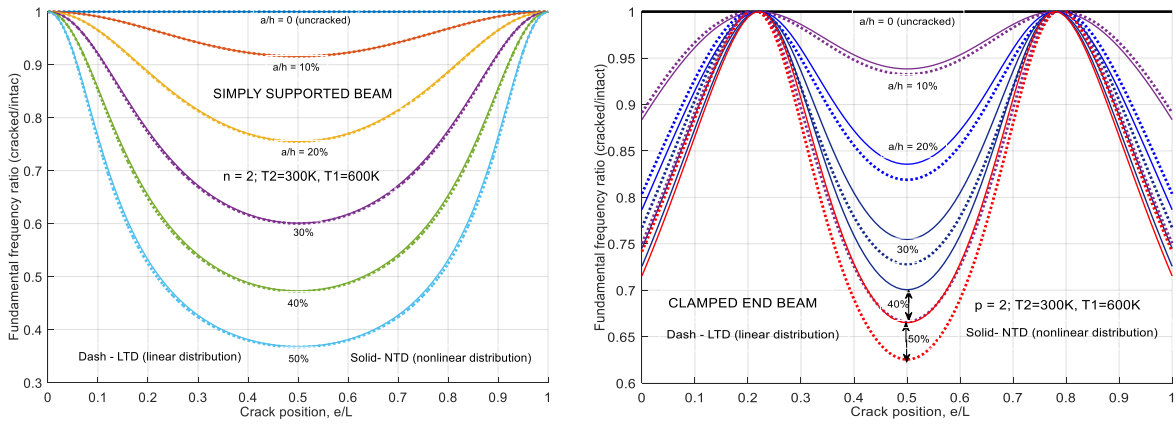

(a) SS-beam (b) CC-beam

Fig. 10. Effect of linear and nonlinear temperature rise distributions on sensitivity of fundamental bending frequency to crack

as the ratio of cracked and intact beam frequencies is unchanged due to the thermal effect. This is like the longitudinal frequency, when material and temperature equally affect the frequencies of cracked and intact beams. So, the effect of the material gradation index and temperature on the bending frequencies could not be investigated by using the above-introduced sensitivity. It should be examined by directly solving Eq. (43), the numerical solutions of which, represented through the nondimensional frequency $\bar{\omega} = (L^2/h)\sqrt{(\rho_b/E_b)}$, are presented in Figs. 11 and 12. Obviously, an increase in the material gradation index and temperature leads to a monotonic reduction of the bending frequency but it does not change the frequency variation against crack location. Nevertheless, as mentioned above, both material gradation and temperature may increase the sensitivity of the natural frequencies to crack depth.

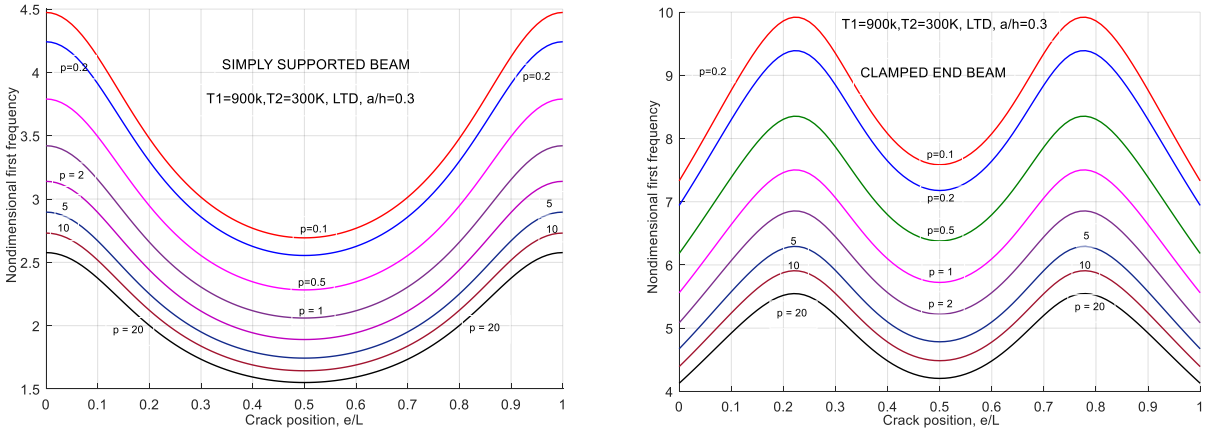

(a) SS-beam (b) CC-beam

Fig. 11. Fundamental bending frequency versus crack position in various material distribution index, $T_2 = 300$ K, $T_1 = 900$ K, LTD, $a/h = 0.3$

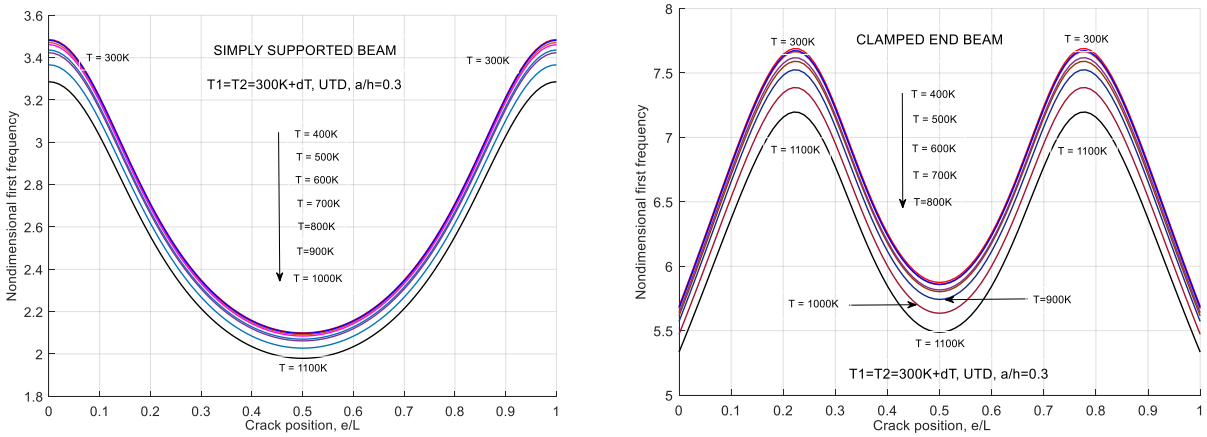

(a) SS-beam (b) CC-beam

Fig. 12. Fundamental frequency of bending vibration versus crack position in various generic temperatures of UTD, d$T = 100$ K, $T_2 = 300$ K

5. CONCLUSIONS

In this paper, a specific model of cracked temperature-dependent functionally graded beams is conducted with the aim of investigating uncoupled axial and flexural vibrations of the beams depending on the material gradient index, temperature rise and crack parameters. The power law of material gradation is assumed, the Euler–Bernoulli beam theory is adopted, and the Hamilton principle is applied for establishing equations of motion that allow the axial and flexural vibration modes to be decoupled. Transverse open cracks are modeled by a pair of springs, the compliances of which are calculated from the crack depth. The longitudinal wave speed and fundamental frequency in the axial and flexural vibrations are examined along the material gradient index, temperature rise distributions, and crack depth and locations. The numerically computed results show a monotonic reduction of the wave speed and natural frequencies with an increasing material gradient index, temperature rise and crack depth. Crack location-induced changes in the axial and flexural vibration frequencies are like those obtained for temperature-independent functionally graded beams.

DECLARATION OF COMPETING INTEREST

The authors declare that they have no known competing financial interests or personal relationships that could have appeared to influence the work reported in this paper.

CREDIT AUTHOR STATEMENT

Do Nam: *Resources, Validation, Writing - Review & Editing*. Nguyen Tien Long: *Investigation, Software, Writing - Original Draft*. Phi Thi Hang: *Formal analysis, Data Curation, Visualization*. Nguyen Tien Khiem: *Conceptualization, Methodology, Supervision, Project administration*.

FUNDING

This study is financially supported by Vietnam Foundation for Science and Technology Development, NAFOSTED under Grant of number 107.01-2025.20.

REFERENCES

Alshorbagy, A. E. (2013). Temperature effect on the vibration characteristics of a functionally graded thick beam. *Ain Shams Engineering Journal*, *4*(3), 455–464. https://doi.org/10.1016/j.asej.2012.11.001

Aria, A., Friswell, M., & Rabczuk, T. (2019). Thermal vibration analysis of cracked nanobeams embedded in an elastic matrix using finite element analysis. *Composite Structures*, *212*, 118–128. https://doi.org/10.1016/j.compstruct.2019.01.040

Aydin, K. (2013). Free vibration of functionally graded beams with arbitrary number of surface cracks. *European Journal of Mechanics A/Solids*, *42*, 112–124. https://doi.org/10.1016/j.euromechsol.2013.05.002

Aydogdu, M., & Taskin, V. (2007). Free vibration analysis of functionally graded beams with simply supported edges. *Materials and Design*, *28*(5), 1651–1656. https://doi.org/10.1016/j.matdes.2006.02.007

Birman, V., & Byrd, L. M. (2007). Modeling and analysis of functional graded materials and structures. *Applied Mechanics Reviews*, *60*(5), 195–216. https://doi.org/10.1115/1.2777164

Chen, J., Fang, H., Liu, W., Zhu, L., Zhuang, Y., Wang, J., & Han, J. (2018). Thermal vibration of FGM beams with general boundary conditions using a higher-order shear deformation theory. *Composites Part B: Engineering*, *153*, 376–386. https://doi.org/10.1016/j.compositesb.2018.08.122

Chen, W. R., & Chang, H. (2017). Closed-form solution for free vibration frequencies of functionally graded Euler-Bernoulli beams. *Mechanics of Composite Materials*, *53*(1), 79–98. https://doi.org/10.1007/s11029-017-9642-3

Chondros, T. G., Dimarogonas, A. D., & Yao, J. (1998a). A continuous cracked beam vibration theory. *Journal of Sound and Vibration*, *215*(1), 17–34. https://doi.org/10.1006/jsvi.1998.1640

Chondros, T. G., Dimarogonas, A. D., & Yao, J. (1998b). Longitudinal vibration of a continuous cracked bar. *Engineering Fracture Mechanics*, *61*(5-6), 593–606. https://doi.org/10.1016/s0013-7944(98)00071-x

Elaikh, T. E., & Agboola, O. O. O. (2022). Investigation of transverse vibration characteristics of cracked axially moving functionally graded beam under thermal load. *Trends in Sciences*, *19*(23), 1349. https://doi.org/10.48048/tis.2022.1349

Esen, I., Özarpa, C., & Eltaher, M. A. (2021). Free vibration of a cracked FG microbeam embedded in an elastic matrix and exposed to magnetic field in a thermal environment. *Composite Structures*, *261*, 113552. https://doi.org/10.1016/j.compstruct.2021.113552

Gayen, D. (2024). Thermo-elastic buckling and free vibration behavior of functionally graded beams with various materials gradation laws. *International Journal on Interactive Design and Manufacturing*, *19*(7), 5397–5416. https://doi.org/10.1007/s12008-024-02141-1

Gayen, D., Tiwari, R., & Chakraborty, D. (2019). Static and dynamic analyses of cracked functionally graded structural components: A review. *Composites Part B: Engineering*, *173*, 106982. https://doi.org/10.1016/j.compositesb.2019.106982

Gupta, M., & Talha, M. (2015). Recent development in modeling and analysis of functionally graded materials and structures. *Progress in Aerospace Sciences*, *79*, 1–14. https://doi.org/10.1016/j.paerosci.2015.07.001

Hai, T. T., Hang, P. T., Botyan, S., & Khiem, N. T. (2025). The effect of neutral axis position on fundamental frequency of functionally graded Timoshenko beams in nonlinear temperature rise environment. *Journal of Thermal Stresses*, *48*(4), 376–399. https://doi.org/10.1080/01495739.2025.2461521

Huyen, N. N., et al. (2025). Coupled effect of crack and temperature on free vibration of functionally graded beams [Accepted]. *Journal of the Brazilian Society of Mechanical Sciences and Engineering*.

Huyen, N. N., & Khiem, N. T. (2017). Modal analysis of functionally graded Timoshenko beam. *Vietnam Journal of Mechanics*, *39*(1), 31–50. https://doi.org/10.15625/0866-7136/7582

Jin, C., & Wang, X. (2015). Accurate free vibration analysis of Euler functionally graded beams by the weak form quadrature element method. *Composite Structures*, *125*, 41–50. https://doi.org/10.1016/j.compstruct.2015.01.039

Khiem, N. T., Huyen, N. N., & Long, N. T. (2017). Vibration of cracked Timoshenko beam made of functionally graded material. In *Shock & vibration, aircraft/aerospace, energy harvesting, acoustics & optics, volume 9* (pp. 133–143). River Publishers. https://doi.org/10.1007/978-3-319-54735-0_15

Khiem, N. T., & Lien, T. V. (2001). A simplified method for natural frequencies of multiple cracked beams. *Journal of Sound and Vibration*, *245*(4), 737–751. https://doi.org/10.1006/jsvi.2001.3585

Khiem, N. T. (2022). Vibration of cracked functionally graded beams: General solution and application - a review. *Vietnam Journal of Mechanics*, *44*(4), 317–347. https://doi.org/10.15625/0866-7136/17986

Li, X. F. (2008). A unified approach for analyzing static and dynamic behaviors of functionally graded Timoshenko and Euler-Bernoulli beams. *Journal of Sound and Vibration*, *318*(4-5), 1210–1229. https://doi.org/10.1016/j.jsv.2008.04.056

Mahi, A., Adda Bedia, E., Tounsi, A., & Mechab, I. (2010). An analytical method for temperature-dependent free vibration analysis of functionally graded beams with general boundary conditions. *Composite Structures*, *92*(8), 1877–1887. https://doi.org/10.1016/j.compstruct.2010.01.010

Minh, P. P., & Duc, N. D. (2021). The effect of cracks and thermal environment on free vibration of FGM plates. *Thin-Walled Structures*, *159*, 107291. https://doi.org/10.1016/j.tws.2020.107291

Natarajan, S., et al. (2011). Linear free flexural vibration of cracked functionally graded plates in thermal environment. *Computers & Structures*, *89*, 1535–1546. https://doi.org/10.1016/j.compstruc.2011.04.002

Pradhan, K. K., & Chakraverty, S. (2013). Free vibration of Euler and Timoshenko functionally graded beams by Rayleigh-Ritz method. *Composites Part B: Engineering*, *51*, 175–184. https://doi.org/10.1016/j.compositesb.2013.02.027

Sherafatnia, K., Farrahi, G. H., & Faghidian, S. A. (2014). Analytic approach to free vibration and buckling analysis of functionally graded beams with edge cracks using four engineering beam theories. *International Journal of Engineering*, *27*(6 (C)), 979–990. https://doi.org/10.5829/idosi.ije.2014.27.06c.17

Singh, R., & Sharma, P. (2019). A review on modal characteristics of FGM structures. *1st international conference on advances in mechanical engineering and nanotechnology (ICAMEN 2019)*, *2148*(1), 030037. https://doi.org/10.1063/1.5123959

Su, H., & Banerjee, J. R. (2015). Development of dynamic stiffness method for free vibration of functionally graded Timoshenko beams. *Computers and Structures*, *147*, 107–116. https://doi.org/10.1016/j.compstruc.2014.10.001

Trinh, L. C., Vo, T. P., Thai, H.-T., & Nguyen, T.-K. (2016). An analytical method for the vibration and buckling of functionally graded beams under mechanical and thermal loads. *Composites Part B: Engineering*, *100*, 152–163. https://doi.org/10.1016/j.compositesb.2016.06.067

Yang, J., & Chen, Y. (2008). Free vibration and buckling analyses of functionally graded beams with edge cracks. *Composite Structures*, *83*(1), 48–60. https://doi.org/10.1016/j.compstruct.2007.03.006

Zahedinejad, P., Zhang, C., Zhang, H., & Ju, S. (2020). A comprehensive review on vibration analysis of functionally graded beams. *International Journal of Structural Stability and Dynamics*, *20*(04), 2030002. https://doi.org/10.1142/s0219455420300025

APPENDIX A. CALCULATION OF THERMAL-MECHANICAL CONSTANTS

First, using the expression

$$E(z,T) = E_b(T) + [E_t(T) - E_b(T)]V^p(z), \tag{A.1}$$

where

$$V(z) = \left(\frac{z}{h} + \frac{1}{2}\right), \; E_b(T) = E_0^b(1 + E_1^b T + E_2^b T^2 + E_3^b T^3), \; E_t(T) = E_0^t(1 + E_1^t T + E_2^t T^2 + E_3^t T^3), \tag{A.2}$$

with the coefficients $E_k^t, E_k^b, k = 0,1,2,3$ given in Table 1 for the chosen top and bottom materials. The latter expressions allow one to calculate

$$E_t(T) - E_b(T) = E_0^{(t-b)}(1 + E_1^{(t-b)} T + E_2^{(t-b)} T^2 + E_3^{(t-b)} T^3), \tag{A.3}$$

where the following notations are used

$$E_0^{(t-b)} = E_0^t - E_0^b, \quad E_k^{(t-b)} = (E_0^t E_k^t - E_0^b E_k^b)/E_0^{(t-b)}, \quad k = 1,2,3.$$

Substituting Eqs. (A.2) and (A.3) into Eq. (A.1) allows one to express Eq. (19) as

$$\begin{aligned} E(z,T) &= [\bar{E}_0^b + \bar{E}_0^{(t-b)} V^p(z)] + [\bar{E}_1^b + \bar{E}_1^{(t-b)} V^p(z)]T(z) \\ &\quad + [\bar{E}_2^b + \bar{E}_2^{(t-b)} V^p(z)]T^2(z) + [\bar{E}_3^b + \bar{E}_3^{(t-b)} V^p(z)]T^3(z), \\ \bar{E}_0^b &= E_0^b, \quad \bar{E}_0^{(t-b)} = E_0^{(t-b)}, \quad \bar{E}_k^b = E_0^b E_k^b, \quad \bar{E}_k^{(t-b)} = E_0^t E_k^t - E_0^b E_k^b, \quad k = 1,2,3. \end{aligned} \tag{A.4}$$

Furthermore, using the following expressions

$$T(z) = T_b + (T_t - T_b)\delta T(z) = T_b + T_{(t-b)}\delta T(z), \quad T_{(t-b)} = T_t - T_b,$$

with

$$\delta T(z) = \frac{1}{C}\sum_{n=0}^{N} \frac{(-1)^n}{np+1}\left[\frac{k_t - k_b}{k_b}\right]^n \left(\frac{z}{h} + \frac{1}{2}\right)^{np+1}, \quad C = \int_{-h/2}^{h/2} \frac{\mathrm{d}z}{k(z)} = \sum_{n=0}^{N} \frac{(-1)^n}{np+1}\left[\frac{k_t - k_b}{k_b}\right]^n,$$

one obtains

$$E(z,T) = \sum_{k=0}^{3} \sum_{n_1,\ldots,n_k=0}^{N} \delta_{n_1} \ldots \delta_{n_k} [\bar{E}_k^b V^{m_k}(z) + \bar{E}_k^{(t-b)} V^{m_k+p}(z)], \tag{A.5}$$

where the following notations have been introduced

$$\delta_n = \frac{(-1)^n}{(np+1)C}\left[\frac{k_t - k_b}{k_b}\right]^n,$$

$$m_0 = 0, \quad m_1 = np+1, \quad m_2 = (n_1+n_2)p+2, \quad m_3 = (n_1+n_2+n_3)p+3.$$

Using Eq. (A.5), one can calculate the integrals

$$\begin{aligned} \int_{-h/2}^{h/2} E(z,T)\mathrm{d}z &= h\psi_0(p, \bar{E}_0^t, \bar{E}_0^b, \ldots, \bar{E}_3^t, \bar{E}_3^b), \\ \int_{-h/2}^{h/2} E(z,T)z\mathrm{d}z &= h^2\psi_1(p, \bar{E}_0^t, \ldots, \bar{E}_3^t, \bar{E}_0^b, \ldots, \bar{E}_3^b), \\ \int_{-h/2}^{h/2} E(z,T)z^2\mathrm{d}z &= h^3\psi_2(p, \bar{E}_0^t, \ldots, \bar{E}_3^t, \bar{E}_0^b, \ldots, \bar{E}_3^b), \end{aligned} \tag{A.6}$$

where

$$\psi_0(p, E_t, E_b) = \sum_{k=0}^{3} \sum_{n_1,\ldots,n_k=0}^{\infty} \delta_{n_1} \ldots \delta_{n_k} \left[\frac{\bar{E}_k^b}{m_k+1} + \frac{\bar{E}_k^{(t-b)}}{m_k+1+p}\right], \tag{A.7a}$$

$$\psi_1(p,E_t,E_b)=\frac{1}{2}\sum_{k=0}^{3}\sum_{n_1,\ldots,n_k=0}^{\infty}\delta_{n_1}\ldots\delta_{n_k}\left[\frac{m_k\bar{E}_k^b}{(m_k+1)(m_k+2)}+\frac{(m_k+p)\bar{E}_k^{(t-b)}}{(m_k+1+p)(m_k+2+p)}\right], \tag{A.7b}$$

$$\psi_2(p,E_t,E_b)=\frac{1}{4}\sum_{k=0}^{3}\sum_{n_1,\ldots,n_k=0}^{\infty}\delta_{n_1}\ldots\delta_{n_k}\left[\begin{array}{l}\dfrac{(m_k^2+m_k+2)\bar{E}_k^b}{(m_k+1)(m_k+2)(m_k+3)}\\ +\dfrac{[(m_k+p)^2+(m_k+p)+2]\bar{E}_k^{(t-b)}}{(m_k+1+p)(m_k+2+p)(m_k+3+p)}\end{array}\right]. \tag{A.7c}$$

Using the calculated integrals,

$$\begin{aligned}\int_{-h/2}^{h/2}V^m(z)\mathrm{d}z&=\int_{-h/2}^{h/2}\left(\frac{z}{h}+\frac{1}{2}\right)^m\mathrm{d}z=h\int_0^1 y^m\mathrm{d}y=\frac{h}{m+1},\\ \int_{-h/2}^{h/2}V^m(z)z\mathrm{d}z&=\int_{-h/2}^{h/2}\left(\frac{z}{h}+\frac{1}{2}\right)^m z\mathrm{d}z=h^2\int_0^1 y^m\left(y-\frac{1}{2}\right)\mathrm{d}y=\frac{h^2m}{2(m+1)(m+2)},\\ \int_{-h/2}^{h/2}V^m(z)z^2\mathrm{d}z&=\int_{-h/2}^{h/2}\left(\frac{z}{h}+\frac{1}{2}\right)^m z^2\mathrm{d}z=h^3\int_0^1 y^m\left(y-\frac{1}{2}\right)^2\mathrm{d}y=\frac{h^3(m^2+m+2)}{4(m+1)(m+2)(m+3)},\end{aligned} \tag{A.8}$$

the exact position of the neutral axis (4) and the thermal-mechanical constants (9) can be calculated as follows:

$$\bar{h}_0=\frac{h_0}{h}=\frac{\displaystyle\sum_{m=0}^{3}\frac{(m+1)(m+2)(m+p)\bar{E}_m^t-p(2-m^2-mp)\bar{E}_m^b}{2(m+1)(m+2)(m+p+1)(m+p+2)}}{\displaystyle\sum_{m=0}^{3}\frac{(m+1)\bar{E}_m^t+p\bar{E}_m^b}{(m+1)(m+1+p)}}; \tag{A.9}$$

$$\begin{aligned}A_{11}&=b\int_{-h/2}^{h/2}E(z,T)\mathrm{d}z=bh\psi_0(p,\bar{E}_0^t,\bar{E}_0^b,\ldots,\bar{E}_3^t,\bar{E}_3^b),\\ A_{12}&=0,\quad A_{22}=bh^3[\psi_2-2\bar{h}_0\psi_1+\bar{h}_0^2\psi_0],\end{aligned} \tag{A.10}$$

with the coefficients $\bar{E}_0^t,\bar{E}_0^b,\ldots,\bar{E}_3^t,\bar{E}_3^b$ given above in Eq. (A.4).

Similarly, the temperature-independent constants I_{11},I_{12},I_{22} can be calculated as follows:

$$\begin{aligned}I_{11}&=\frac{bh(\rho_t+p\rho_b)}{p+1},\quad I_{12}=\frac{bh^2}{p+1}\left[\frac{p(\rho_t-\rho_b)}{2(p+2)}-\bar{h}_0(\rho_t+p\rho_b)\right],\\ I_{22}&=\frac{bh^3}{12(p+1)}\left[\frac{p(p^2+3p+8)\rho_b}{(p+2)(p+3)}-\frac{12p(\rho_t-\rho_b)\bar{h}_0}{p+2}+12(\rho_t+p\rho_b)\bar{h}_0^2\right].\end{aligned} \tag{A.11}$$

Now we are going to calculate the coefficient of thermal expansion

$$A_T=b\int_{-h/2}^{h/2}E(z,T)\alpha(z,T)\Delta T\mathrm{d}z,\quad \Delta T=T(z)-T_0.$$

Using the following relations

$$\alpha_b(T)=\alpha_0^b(1+\alpha_1^bT),\quad \alpha_t(T)=\alpha_0^t(1+\alpha_1^tT),\quad T(z)=T_b+(T_t-T_b)\delta T(z)=T_b+T_{(t-b)}\delta T(z),$$

the expression $\alpha(z,T)=\alpha_b(T)+[\alpha_t(T)-\alpha_b(T)]V^p(z)$ can be written in the form

$$\alpha(z,T)=A_0^b+A_0^{(t-b)}V^p+(A_1^b+A_1^{(t-b)}V^p)\delta T, \tag{A.12}$$

where

$$\begin{aligned}&A_0^b=\alpha_0^b(1+\alpha_1^bT_b),\quad A_1^b=\alpha_0^b\alpha_1^bT_{(t-b)},\quad A_0^t=\alpha_0^t(1+\alpha_1^tT_b),\quad A_1^t=\alpha_0^t\alpha_1^tT_{(t-b)},\\ &A_0^{(t-b)}=\alpha_0^{(t-b)}(1+\alpha_1^{(t-b)}T_b)=A_0^t-A_0^b,\quad A_1^{(t-b)}=\alpha_0^{(t-b)}\alpha_1^{(t-b)}T_{(t-b)}=A_1^t-A_1^b.\end{aligned}$$

Now, substituting the expression for $\delta T(z)$ obtained above into Eq. (A.12) yields

$$\alpha(z,T) = A_0^b + A_0^{(t-b)}V^p + \sum_{n=0}^{\infty}\delta_n(A_1^b V^{np+1} + A_1^{(t-b)}V^{np+1+p}). \tag{A.13}$$

Therefore, one can calculate

$$\begin{aligned} A_T &= b\int_{-h/2}^{h/2} E(z,T)\alpha(z,T)\Delta T\mathrm{d}z = b\int_{-h/2}^{h/2} E(z,T)\alpha(z,T)(T-T_b)\mathrm{d}z \\ &= bT_{(t-b)}\int_{-h/2}^{h/2} E(z,T)\alpha(z,T)\delta T(z)\mathrm{d}z \\ &= bhT_{(t-b)}\sum_{r=1}^{5}\sum_{n_1,\ldots,n_r=0}^{\infty}\delta_{n_1}\ldots\delta_{n_r}\left[\frac{R_{r-1}^{bb}}{m_r+1} + \frac{R_{r-1}^{b(t-b)}}{m_r+p+1} + \frac{R_{r-1}^{2(t-b)}}{m_r+2p+1}\right], \end{aligned} \tag{A.14}$$

where the following notations have been introduced

$$\begin{aligned} &R_0^{bb} = A_0^b\bar{E}_0^b, \quad R_0^{b(t-b)} = A_0^{(t-b)}\bar{E}_0^b + A_0^b\bar{E}_0^{(t-b)}, \quad R_0^{2(t-b)} = A_0^{(t-b)}\bar{E}_0^{(t-b)}, \\ &R_1^{bb} = A_0^b\bar{E}_1^b + A_1^b\bar{E}_0^b, \quad R_1^{b(t-b)} = A_0^{(t-b)}\bar{E}_1^b + A_0^b\bar{E}_1^{(t-b)} + A_1^{(t-b)}\bar{E}_0^b + A_1^b\bar{E}_0^{(t-b)}, \\ &R_1^{2(t-b)} = A_0^{(t-b)}\bar{E}_1^{(t-b)} + A_1^{(t-b)}\bar{E}_0^{(t-b)}, \quad R_2^{bb} = A_0^b\bar{E}_2^b + A_1^b\bar{E}_1^b, \\ &R_2^{b(t-b)} = A_1^{(t-b)}\bar{E}_1^b + A_1^b\bar{E}_1^{(t-b)} + A_0^{(t-b)}\bar{E}_2^b + A_0^b\bar{E}_2^{(t-b)}, \\ &R_2^{2(t-b)} = A_1^{(t-b)}\bar{E}_1^{(t-b)} + A_0^{(t-b)}\bar{E}_2^{(t-b)}, \quad R_3^{bb} = A_0^b\bar{E}_3^b + A_1^b\bar{E}_2^b, \\ &R_3^{b(t-b)} = A_1^{(t-b)}\bar{E}_2^b + A_1^b\bar{E}_2^{(t-b)} + A_0^{(t-b)}\bar{E}_3^b + A_0^b\bar{E}_3^{(t-b)}, \\ &R_3^{2(t-b)} = A_1^{(t-b)}\bar{E}_2^{(t-b)} + A_0^{(t-b)}\bar{E}_3^{(t-b)}, \\ &R_4^{bb} = A_1^b\bar{E}_3^b, \quad R_4^{b(t-b)} = A_1^{(t-b)}\bar{E}_3^b + A_1^b\bar{E}_3^{(t-b)}, \quad R_4^{2(t-b)} = A_1^{(t-b)}\bar{E}_3^{(t-b)}, \\ &m_1 = np+1, \quad m_2 = (n_1+n_2)p+2, \quad m_3 = (n_1+n_2+n_3)p+3, \\ &m_4 = (n_1+n_2+n_3+n_4)p+4, \quad m_5 = (n_1+n_2+n_3+n_4+n_5)p+5. \end{aligned} \tag{A.15}$$